Self-Assembly of Complex Vesicles

G. J. A. Sevink*,† and A. V. Zvelindovsky*,‡

Leiden Institute of Chemistry, Leiden University, PO Box 9502, 2300 RA Leiden, The Netherlands, and Centre for Materials Science, Department of Physics, Astronomy and Mathematics, University of Central Lancashire, Preston PR1 2HE, United Kingdom

Received April 1, 2005; Revised Manuscript Received June 13, 2005

ABSTRACT: We demonstrate the full kinetic pathways of self-assembly of polymeric amphiphiles into a rich variety of complex vesicles by large-scale computer simulations based on dynamic self-consistent-field theory. The vesicular nanostructure can be tailored by both kinetic and thermodynamic factors.

Introduction

Understanding the principles of vesicle evolution is key to the understanding of many cellular processes in biology as well as the design and function of self-assembled synthetic vesicles for nanotechnology.[1−4] In biology, lipid membrane fusion and fission are fundamental in processes ranging from fertilization, synapse release, intercellular traffic, and viral infection.[5,6] It was recently shown that block copolymers are also capable of forming vesicles, so-called polymersomes, which are in general much more stable than lipidic vesicles.[7,8] Since polymersomes have been prepared from a wide range of polymers with intricate properties, they are potentially interesting systems for nanotechnological application such as targeted drug-release capsules and microreactors.

The amphiphilic nature of synthetic or biological molecules is defined by its architecture, which consists of a hydrophobic and a hydrophilic part. When added to solvent, amphiphilic molecules align according to well-defined patterns and give rise to pluriform aggregates. The morphology of the aggregates is determined by the amphiphilic molecular architecture as well as the nature of the solvent. Scanning electron microscopy and scattering methods have revealed various morphologies: spherical micelles, micellar rods, bilayers, vesicles, and inverted aggregates.[7]

The basic physical mechanisms in cellular membrane fusion and fission are not well understood. There is some understanding that the pathways in many biological membranes are essentially lipidic in nature.[5,6] A consequence of this finding is the reductionist approach in which synthetic amphiphilic membranes could serve as a scaffold for the understanding of the morphological processes in biological systems, which generally consist of a wide variety of compounds.

Self-organization of amphiphilic molecules into membranes and vesicles is long seen as a complex interplay between kinetic and thermodynamic factors.[1] While the thermodynamic factor is well studied,[4] the kinetic factor is subject to ongoing debate.[2,3] For lipids it was very recently decisively concluded that the spontaneous formation of vesicles is a kinetic rather than thermodynamic controlled process.[2,3] For polymeric vesicles it was suggested that they can be thermodynamically stable rather then metastable, exemplary of the fact that the situation for block copolymer vesicles is far less clear. Recently, much effort has been devoted to the analysis of vesicle formation[9−16] and fusion[17−22] by computer simulation. It should be noted that, especially in the fusion studies, the observed phenomena suffer from uncertainty due to the particular constraints (imposed stresses or enforced bilayer contacts) adapted in the different modeling approaches in order to initiate the fusion process.

We argue that large-scale simulation, where multiple vesicle formation and fusion can be observed, is essential for the description of the evolution of a system with many metastable states. Modern supercomputers do not allow achieving this result with particle-based methods. Particle-based methods (both dynamical and Monte Carlo) have been able to simulate some separate steps of vesicle formation and evolution, but the time ranges and system sizes accessible by the methods are still far beyond those needed to realistically model experimental situations.[8,23] In particular, the simulation of a complete pathway from a homogeneous molecule mixture to vesicle fusion with all distinctive steps in one computer run is not accessible by these methods. The most advanced are aimed at modeling isolated events; they are able to describe the dynamics of one or at most two small vesicles in a simulation volume. Coarse-grained field methods, allowing for the simulation of larger volumes, are promising solutions.

Very recently, a self-consistent-field theory (SCFT) was applied to study vesicles and vesicular aggregates in two dimensions (2D).[24] However, in addition to the results being limited to two dimensions, this SCFT calculation did not allow for the investigation of kinetic pathways of vesicle formation.[24] Here we report the results of large-scale three-dimensional (3D) dynamic SCFT computer simulations of hierarchical self-assembly of polymeric amphiphiles, following the pathways from a complete mixture of molecules to the formation of large colonies of complex vesicles (like uni- and multilayered vesicles, toroids, helicoids, etc.). Our method combines thermodynamics and kinetics, by minimizing a free energy for an ensemble of model molecules following the dynamics of the coarse-grained amphiphile density distributions, which effectively averages the movement of individual molecules. Our results offer evidence that many complex vesicles can be thermodynamically metastable structures. The vesicular shape is very diverse and sensitive to a complex interplay of two kinetic processes: macrophase

† Leiden University.
‡ University of Central Lancashire.

10.1021/ma0506740 CCC: $30.25
Published on Web 07/29/2005

separation of amphiphiles from solvent and microphase separation between amphiphilic molecular blocks.

Results and Discussion

Computer simulations were performed with the in-house developed parallel code based on dynamic SCFT and extensively described in the literature earlier. We provide a short description of this theory (for details see ref 25). We model the pattern formation that occurs when a block copolymer solution is brought into a state where the chemically different blocks phase separate on a mesoscopic level (1−1000 nm). In our model, a block copolymer molecule is represented by a Gaussian chain consisting of N beads. Each bead typically represents a number of chemically similar monomers; different bead types denote differences in chemical monomeric nature. The mapping of actual polymers onto this Gaussian chain representation is extensively discussed elsewhere. The block copolymer amphiphiles studied here are modeled as A_iB_j Gaussian chains (with variable i and j) in one-bead solvent (S). The three-dimensional volume of the simulated system is denoted by V and contains n_p polymer chains and n_s solvent chains. The interchain interactions are incorporated via a mean field with interaction strength controlled by the value of ϵ_{IJ} (I, J = A, B, or S); positive values denote repulsion and negative attraction. They are directly related to the familiar Flory−Huggins parameters χ_{IJ} (see below). The microstructure patterns are described by the coarse-grained variables, which are the density fields $\rho_I(r)$ of the different species I. Given these density fields, a free energy functional $F[\rho]$ can be defined as follows:

$$F[\rho] = -kT \ln \frac{\Phi^{n_p}\Phi^{n_s}}{n_p!n_s!} - \sum_I \int_V U_I(\mathbf{r})\, \rho_I(\mathbf{r})\, d\mathbf{r} + F^{mid}[\rho] \quad (1)$$

Here Φ is the intramolecular partition function for the ideal Gaussian chain in the external field U_I, and F^{mid} is the contribution due to the nonideal mean-field interactions. The external potentials U_I and the density fields ρ_I are bijectively related in a self-consistent way via a density functional for Gaussian chains.

Several methods can be employed to search for the minimum of free energy (1) and equilibrium density field $\rho_I(r)$. They can roughly be divided into *static* and *dynamic* methods. In this article, we use a dynamic scheme that has the advantage that it intrinsically considers dynamic pathways towards a free energy minimum, including visits to long-living metastable states. In this sense, the model can be seen to mimic the experimental reality when compared to static or quasi-dynamic schemes, which are optimizations, based upon mathematical arguments. The thermodynamic forces driving the pattern formation in time are the gradients of the chemical potential $\mu_I(r) = \delta F/\delta\rho_I$, and the pattern evolution is described by

$$\frac{\partial \rho_I}{\partial t} = M_I \nabla \rho_I \nabla \mu_I + \eta_I \quad (2)$$

where M_I is a constant mobility for bead I and $\eta_I(r)$ is a noise field, distributed according to the fluctuation−dissipation theorem. During the simulation, the dynamics of the density distribution is followed, which effectively averages over the individual molecules. Each large-scale simulation took ∼20 h CPU time per processor on 32 processors of a SGI Origin 3800 supercomputer.

Lamellar Elipsoids, Helicoids, Platelets, and Others. Before performing a large-scale simulation, one needs to determine the range of parameters suitable for vesicle formation. In addition to the variable architecture (the relative length of the blocks) of the amphiphile A_iB_j and amphiphile/solvent composition, we have three interaction parameters: the interaction of A- and B-blocks with the solvent (S) and with each other. These interactions are parametrized by the variable ϵ_{IJ} (I and J denote different bead species); they are related to the familiar Flory−Huggins parameter χ, via the expression $\chi_{IJ} = \beta\epsilon_{IJ}/\nu$ (with $\beta = 1/kT$ and ν is the polymer chain volume). We expect to find the vesicle forming system to develop large single platelets floating in solvent at some stage of its kinetic evolution. As screening of five-dimensional space is too expensive, we fix two parameters, namely the concentration of the amphiphiles in solvent, chosen to be 20 vol % in each simulation, and the B−S interaction (to $\epsilon_{BS} = 7$ kJ/mol). This interaction value is sufficient for macrophase separation of a polymer from the solvent. In addition, we are bounded to the use of only relatively short Gaussian chains for the amphiphiles, fixing the length of the A-block, $i = 2$, as even short chains in a large simulation volume require extreme computational efforts, close to the current limit. We will show at a later stage that a large simulation volume is essential for our observations. For the purpose of screening of the parameter space in a search for a single platelet we can first restrict ourselves to smaller simulation volumes.

Figure 1 shows the results of this parameter search for $j = 3$. All simulations were started from a homogeneous molecular mixture and continued for 6000 dimensionless time steps (TMS). The results have value by themselves, as they not only locate the parameter range in which vesicle formation is possible but also position these vesicles in phase space with respect to other structures, some of which are observed in experiments as well. The search started from a solvent−A-block interaction $\epsilon_{AS} = 8$ kJ/mol, which is again high enough to ensure macrophase separation of the amphiphiles from the solvent, and introduces an asymmetry in the interaction with the solvent. For the study of vesicle formation, the asymmetry is a prerequisite to form bilayers.

First, we focus on the competition of macro- and microphase separation, by only varying the A−B interaction parameter. Below the value $\epsilon_{AB} = 10$ kJ/mol, the system exhibits only macrophase separation in droplets of various sizes and shapes (spheres, cylinders) without any microstructure. Above this value the two blocks of amphiphile molecules microphase separate from each other within the droplets, and the interplay of micro- and macrophase separation leads to a rich variety of nanostructured droplets.

Figure 1b (top) shows that this interplay leads to ellipsoid-like droplets with an internal structure of stacked lamellar disks or slabs (see also Figure 2a). This region of stacked structures extends into the phase space also for somewhat higher solvophobicity of A-block.

Changing either of these parameters has the effect of modifying the shape of the droplets. This shape is mostly ellipsoidal with a long axis coinciding with the

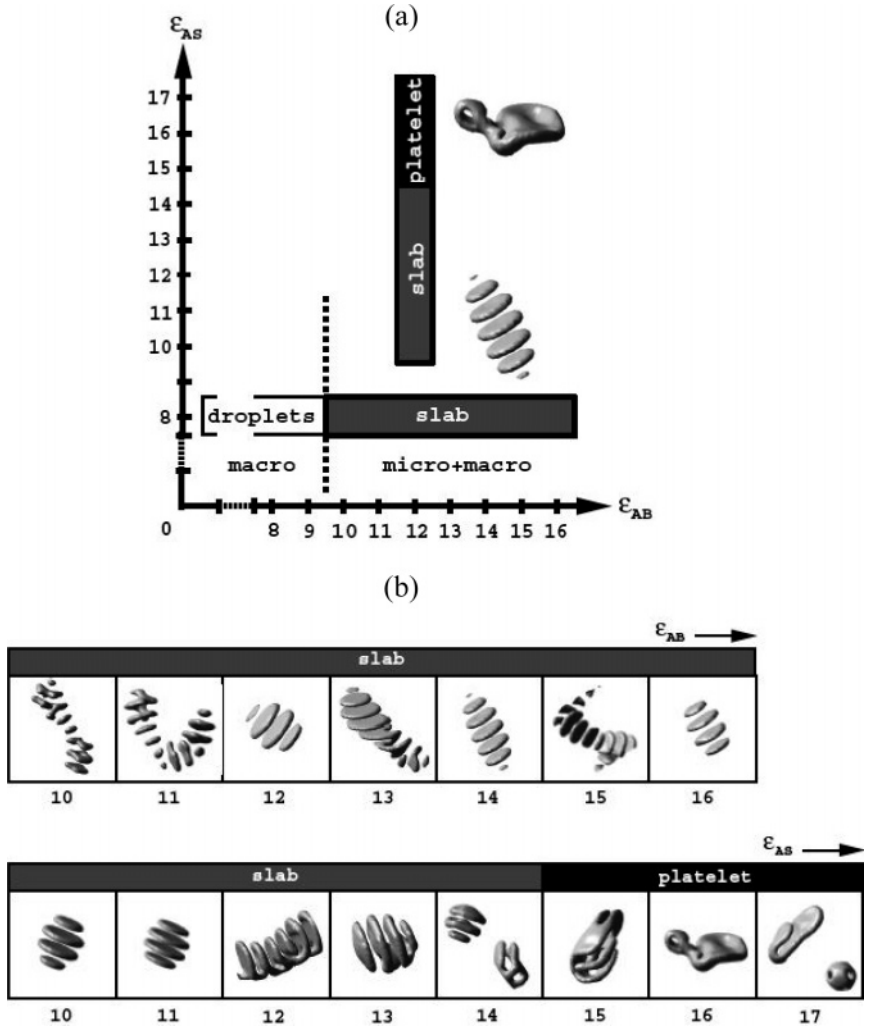

Figure 1. (a) Structures for A_2B_3/solvent mixtures in 32 × 32 × 32 simulation volumes. The interaction parameters of the A-block and the solvent, ϵ_{AS}, and of the A- and B-block, ϵ_{AB}, are given in kJ/mol. (b) Details of the structures (isodensity surfaces of the A-block) Top: structures for the line $\epsilon_{AS} = 8$ kJ/mol. Bottom: structures for the line $\epsilon_{AB} = 12$ kJ/mol.

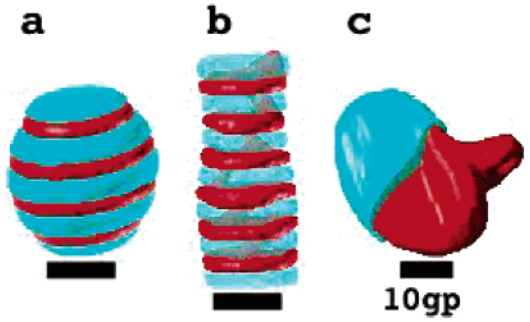

Figure 2. Nanocontainers (red, A-blocks; blue, B-blocks) obtained from simulating 20% amphiphile in a solvent for a A_2B_3 amphiphile in a 32^3 box after 6 × 10^3 TMS. The interaction of the A-block with solvent, ϵ_{AS}, was varied: **a**, 11; **b**, 12; **c**, 16 kJ/mol. The black bar is a reference to the actual size of 10 grid points (gp).

normal to stacked lamellae and the microphase structure perpendicular to the solvent−polymer interface. A deviation of droplets from spheres is a manifestation of nonuniform effective tension along the interface with solvent due to layered structure of the interface. Such lamellar ellipsoids is a common experimental situation observed in lamellar grains and nuclei.[26,27]

An increase of the solvophobicity of the A-block, while keeping the solvent−B-block interaction the same, first drives the system into a stack of lamellar disks spanning the whole simulation volume (Figure 2b). The microphase structure is perpendicular to the solvent−polymer interface, the same as in ellipsoids, but the overall shape of a droplet is cylindrical. The stack is under pressure from the top and bottom due to the periodic boundary conditions and therefore exhibits a well-pronounced screw disclination (see Figure 2b). Similar helical-like structures were experimentally observed in lamellar stacks stretched by a flow.[28,29] Very recent SCFT calculations for a lamellar stack (of somewhat different polymer system) under pressure of the boundary condition of the simulation box show a helixlike structure,[29] similar to ours. The difference with our simulations is that all our structures form spontaneously from an initially homogeneous mixture, while the simulations in ref 29 have been performed for an initially preset cylindrical droplet.

At even stronger solvophobicity of the A-block ($\epsilon_{AS} =$ 16 kJ/mol) the system forms an isolated platelet (Figure 2c). The closure of this large platelet into a vesicle is not observed. The stability of this platelet is an indication of the effect of boundary conditions in the small simulation volumes considered. To reduce these boundary effects, large-scale simulations are essential.

The effect of the periodic boundaries is reduced for smaller object as we can see for the simulated structures

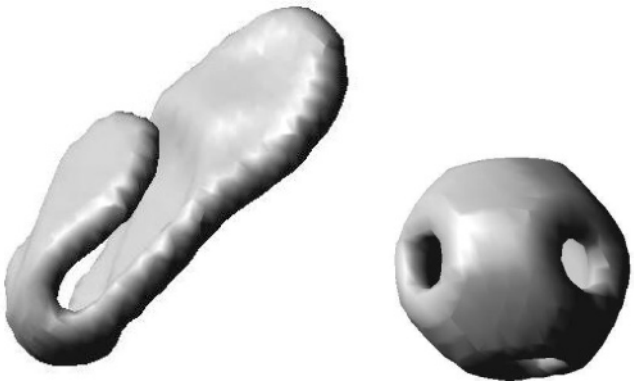

Figure 3. Two disjunct nanostructures (A-blocks) obtained from simulating 20% amphiphile in a solvent, for A_2B_3 amphiphiles in a 32^3 box after 6×10^3 TMS. The lateral extent of the platelet (left) roughly equals that of the simulation volume (32 grid points); the diameter of the perforated onion vesicle (right), containing a micelle in the center (not visible here), is 12 grid points. The interaction of the A-block with solvent ϵ_{AS} = 17 kJ/mol.

shown in Figure 3 for ϵ_{AS} = 17 kJ/mol. Instead of a single large platelet (Figure 2c), a large platelet is formed in combination with a much smaller nanocapsule, which is an onion vesicle with perforations in the outer A-rich shell. The details of the formation of this nanocapsule (not shown here) are very similar to the one observed for large simulation volumes (see later sections).

Unilamellar Vesicles and Onions. After determining the parameter-space range where we expect vesicles most likely to form for an A_2B_3 molecule, we perform a number of simulations in a large simulation volume ($64 \times 64 \times 128$) with a fixed set of interaction parameters. Although we consider bad solvent and limit ourselves to the solvent−polymer interaction range where the diblock copolymer is mostly macrophase separated from the solvent, the A-part is relatively solphophobic and the B-part relatively solphophilic since $\epsilon_{AS} > \epsilon_{BS}$. As a consequence, the A-rich regions in the microstructures shown in the remainder will in many cases be surrounded by a B-rich shell, in such a way that the B-rich shell shields the A-rich regions from contacts with the solvent. Some solvent is present in the microphase-separated structures and is mostly found in B-rich regions. We now focus on the influence of the molecular architecture of the amphiphile. The interactions are kept constant for reasons of computational efficiency; we will only vary the length of the B-block. In many biological membranes the solphophobic (tail) part of the molecules is larger than the solphophilic part (head). Here, we vary the length of the relative solphophilic (head) block instead, as we have a special interest in the fundamentals of experimental polymeric vesicular structures that are much less understood, like the exotic structures observed by the Eisenberg group.[33] Simulations with varying length of the A-block (while keeping the B-block length constant), e.g., for the chains A_6B_2, only resulted in relatively simple vesicular structures from a topological point of view (not shown here), comparable to the ones obtained for A_2B_2. For all variations the value of χN is high enough so the bilayers are well segregated, similar to the previous section (χ is the Flory−Huggins parameter, N is the amphiphile's length).

We start from the simplest possible symmetric molecule, making the B-block a bit shorter. Initially homo-

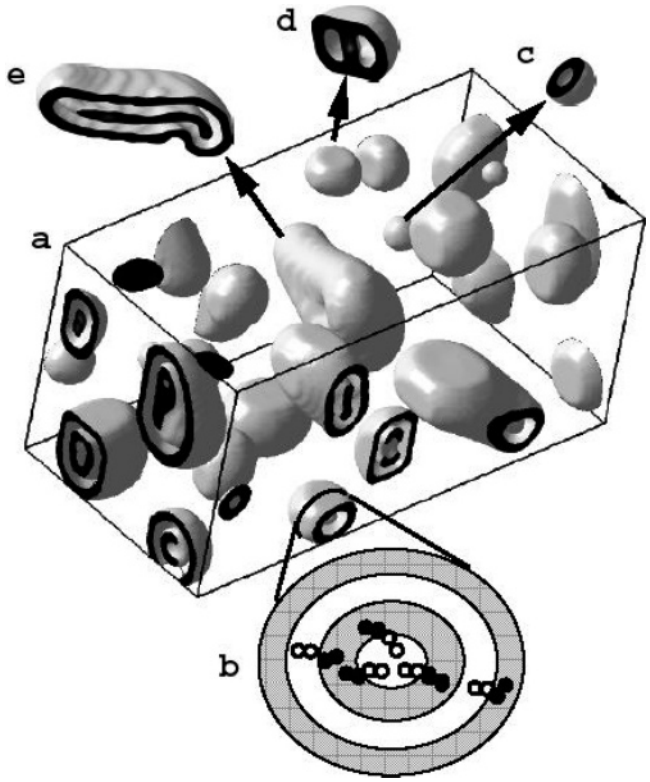

Figure 4. Large-scale simulation of 20% A_2B_2 amphiphile in solvent (S) after 10^4 TMS. The interactions between components are ϵ_{AB} = 12 kJ/mol, ϵ_{AS} = 16 kJ/mol, and ϵ_{BS} = 7 kJ/mol. (**a**) View on the whole $128 \times 64 \times 64$ simulation box (only A-block isosurface shown). (**b**) Schematic representation of all layers in a multilayer vesicle (the amphiphiles are depicted by chains of white (A) and black (B) beads, inside the vesicles the solvent is preferentially located in black regions). (**c**) Zoom and cut through a small unilayer vesicle. (**d**) Zoom and cut through a vesicle with intermembrane neck connection. (**e**) Zoom and cut through a vesicle with encapsulated bilayer sheet.

geneously distributed symmetric A_2B_2 amphiphile molecules self-assemble upon quenching in selective bad solvent into the structures shown in Figure 4. The amphiphile molecules form a bilayer which assembles into vesicles: either unilamellar vesicles (**c**) or multilayer onions (**b**). Characteristic defects, like holes in the inner or outer layers of the vesicles or a neck at the center of a vesicle (**d**), are observed in some members of the vesicle population. In course of time, the vesicles grow and the defects disappear. In some cases long-living elongated vesicles are formed that encapsulate a bilayer sheet (**e**). The latter objects show a tendency to bend, leading to further closure into a large multilayered vesicle; however, the rate at which the closure takes place depends on the initial object size and is significantly lower for larger objects. The time evolution of the system, which leads toward the result in Figure 4, is shown in a series of snapshots in Figure 5 (see also the whole movie in the Supporting Information). Figure 5e, showing the size distribution of the objects at 10000 TMS, illustrates that the majority of objects is still rather small (less than 2 vol %). The size distribution is rather broad, with two small peaks observed at the smallest object size and an intermediate one (around 1 vol %). The mean cluster size is 0.92 vol %. To consider the influence of the polymer concentration on the kinetic pathway of the system, we also performed a short simulation (3000 TMS) for a A_2B_2 system at a lower

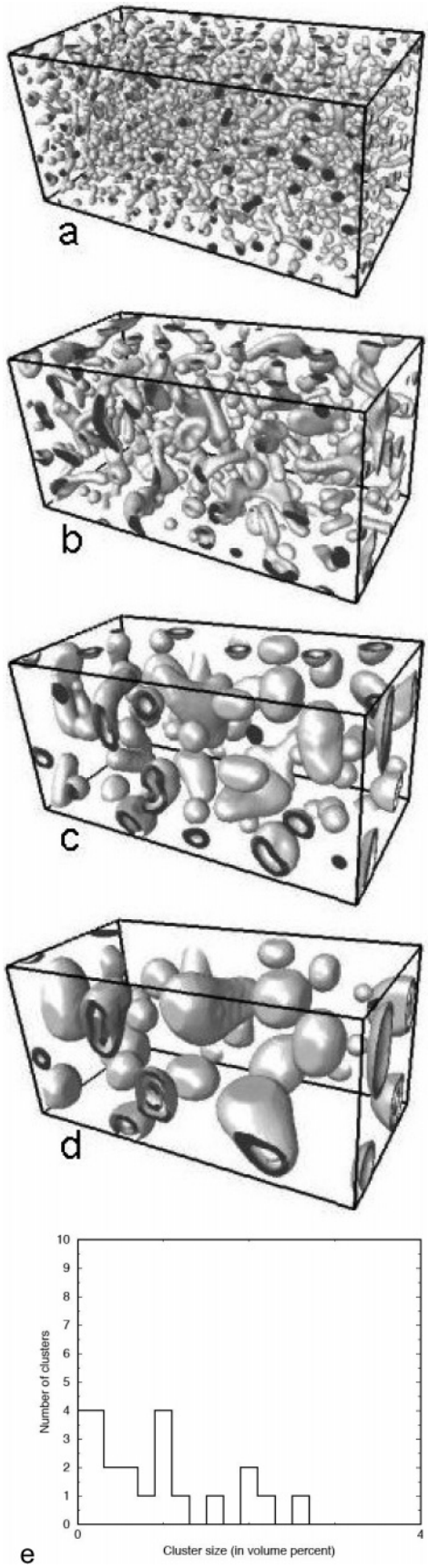

Figure 5. Large-scale simulation of 20% A_2B_2 amphiphile in solvent (S) after (a) 100, (b) 800, (c) 4000, and (d) 10 000 TMS (only A-block isosurface shown). The interactions between components are $\epsilon_{AB} = 12$ kJ/mol, $\epsilon_{AS} = 16$ kJ/mol, and $\epsilon_{BS} = 7$ kJ/mol. In all cases the whole $128 \times 64 \times 64$ simulation box is shown. (e) Number of clusters vs cluster size, in percent of the total simulation volume, for this system (10 000 TMS).

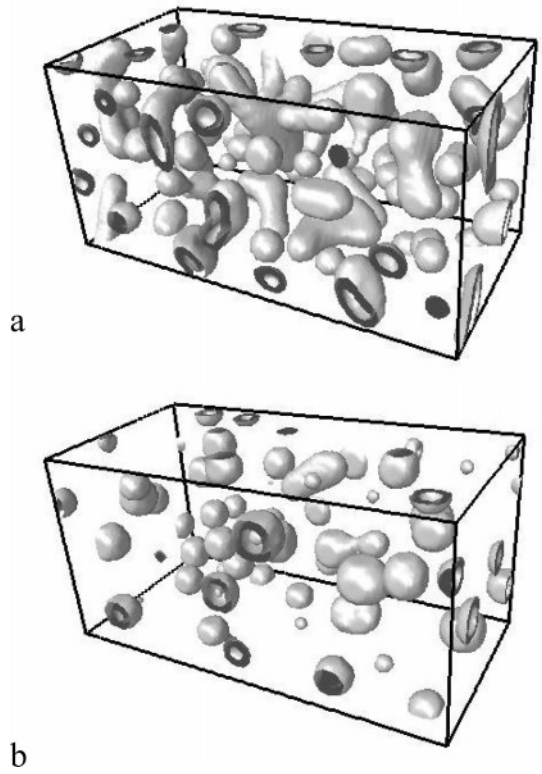

Figure 6. Large-scale simulation of 20% A_2B_2 (a) and 10% A_2B_2 (b) amphiphile in solvent (S) after 3000 TMS (only A-block isosurface shown). The interactions between components are $\epsilon_{AB} = 12$ kJ/mol, $\epsilon_{AS} = 16$ kJ/mol, and $\epsilon_{BS} = 7$ kJ/mol. In both cases the whole $128 \times 64 \times 64$ simulation box is shown.

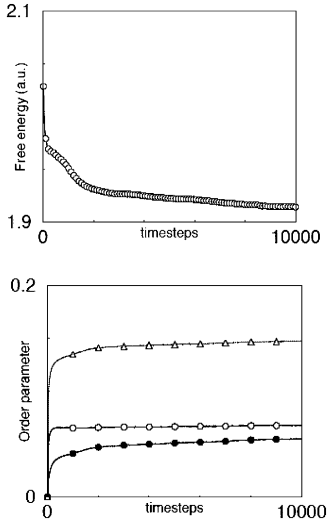

Figure 7. Time evolution of the free energy and segregation parameter $P_I = \int dV\,(\rho_I^2(r)) - (\rho_I^0)^2$ (with ρ_I^0 the mean density of a particular bead type I), for the large-scale simulation shown in Figure 4. The different evolution plots of the segregation parameter are labeled by symbols denoting: A (opaque circles), B (full circles), and S (opaque triangles).

polymer concentration of 10 vol % (Figure 6b). From a direct comparison of the structures at the same time stages in Figures 6a (20 vol %) and 6b, we see that the structures, and therefore the pathways, are rather similar (vesicles). The dynamics in the less concentrated system is however slowed down considerably. The structures are much smaller due to a reduced rate at which existing structures meet and merge to form larger structures, starting from the earliest stages of micelles

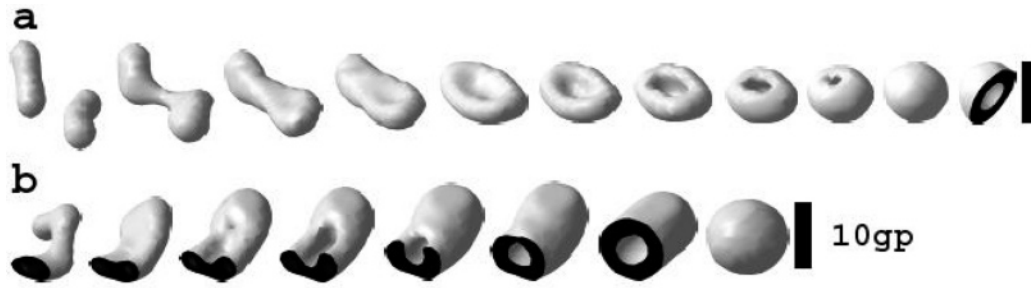

Figure 8. Pathways of unilamellar vesicle formation. The structures are snapshots of two different identified regions in the large system shown in Figure 4. (**a**) Detailed snapshots showing only one vesicle (the final stage of the system is depicted in Figure 4). The time steps are (from left to right, $\times 10^2$) 3, 6, 8, 10, 13, 14, 15, 16, 17, 18, and 18 (cut). (**b**) Same as (**a**), but for a larger vesicle. About one-third of every image is cut to highlight the internal structure. The time steps are (from left to right, $\times 10^2$) 5, 8, 10, 11, 13, 14, 17, and 19. The black bar is a reference to the actual size of 10 grid points (gp).

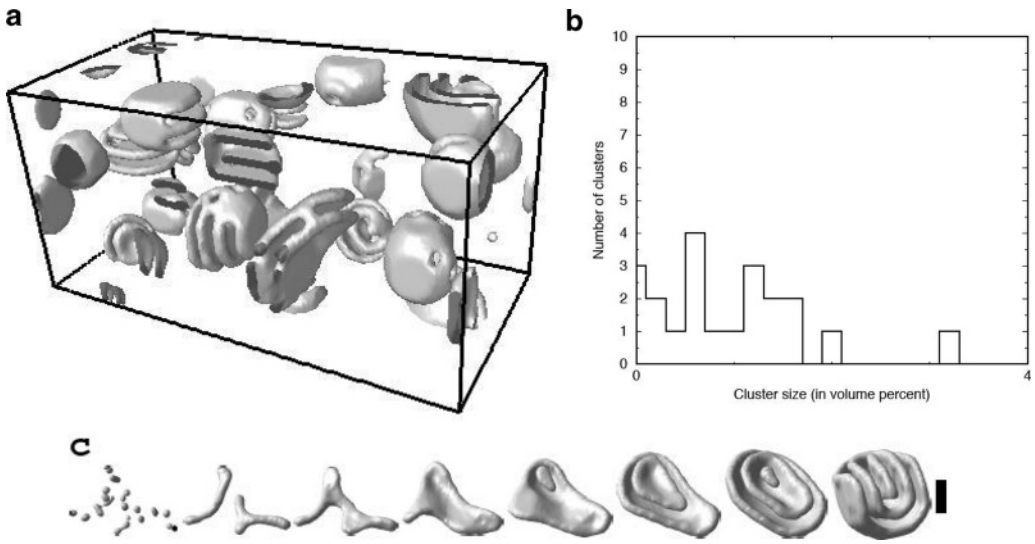

Figure 9. Pathways of multivesicle formation. (a) Simulation result (isosurface of A component at 0.5) after 10^4 simulation steps. (b) Number of clusters vs cluster size, in percent of the total simulation volume, for this system (10^4 TMS). (c) Formation of an onion for this A_2B_3 amphiphile. The parameters and system size are the same as in Figure 4. The time steps are (from left to right, $\times 10^2$) 1, 6, 10, 20, 30, 40, 60, and 100. The black bar is a reference to the actual size of 10 grid points (gp).

and elongated micelles. We therefore conclude that the pathway is, as expected, mainly determined by the material parameters but that the evolution of the size distribution is sensitive to the amount of material and significantly higher for more concentrated systems. Figure 7 shows the free energy of the whole system from Figure 5 and the segregation parameters during the complete process of vesicle formation starting from a homogeneous molecular mixture. The segregation parameters show that after the first and very short stage of phase separation the system reaches a plateau, and further evolution proceeds without much of enrichment of the domains. The decay in the free energy governs the evolution, as seen in Figure 7. We stop the simulation well within the apparent plateau region of the free energy.

The pathway of vesicle formation is unravelled in Figure 8. The initial stage in the self-assembly process is that of spherical micelles (see Figure 5a), similar to the ones shown in the beginning of Figure 9c for the asymmetric A_2B_3 system. Spherical micelles rapidly merge into cylindrical micelles. The cylindrical micelles grow, merge with neighbors, and, at a certain critical size, evolve into energetically favorable disklike or oval platelets. The oval-shaped platelets slowly retract into round disks. The platelets grow until a certain critical size, after which the balance between energy of the rim and bending of a whole platelet favors a closing up of the platelet into a vesicle. Sphere-to-rod and rod-to-vesicle kinetic pathways have recently been observed in a series of experiments for block copolymers in two solvent mixtures.[30,31] Although these systems differ from ours by e.g. the presence of multiple solvents, the details of the experimental pathways agree well with our evolution picture (cf. Figure 3 in ref 31), remarkably including the presence of irregularly shaped or circular lamellae prior to the formation of vesicles. We observe that, depending on the initial size and shape of the platelets, there are two distinct pathways in the closing-up processes. Disk-shaped (or slightly oval) platelets close up directly into a spherical vesicle (Figure 8a). For elongated platelets two kinetic processes (retraction to a disk and closing up) compete, leading to a new pathway. The platelet zips up from the ends (like a sleeping bag) to form a cylindrical vesicle, which consequently retracts as a whole to form a spherical vesicle (Figure 8b). The first two steps, the formation of micelles (spherical and cylindrical) and closure, are comparable in time, while the retraction of a cylindrical vesicle is slower.

We can control the structure of vesicles by choosing an amphiphile's head-to-tail volume ratio. Introducing the asymmetry in the molecular architecture by adding one bead leads to the formation of mostly multilayer vesicles (Figure 9a,c). As the objects are larger when compared to the A_2B_2/solvent system (see Figures 5d

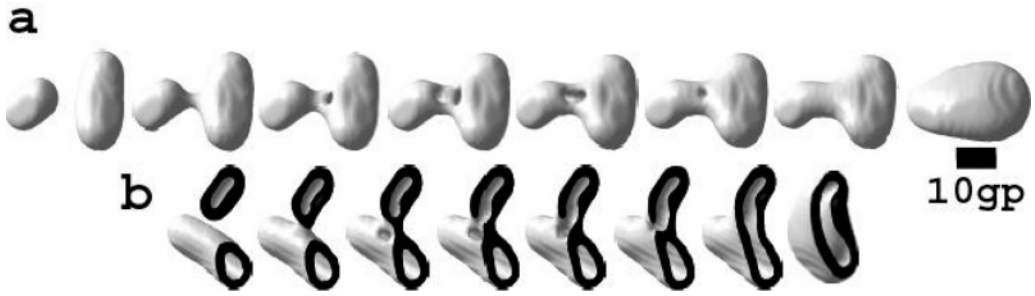

Figure 10. Fusion of vesicles. Snapshots cropped to show only two vesicles (the final stage of the movie is depicted in Figure 4). The time steps are (from left to right, $\times 10^2$) 33, 35, 36, 37, 38, 39, 40, and 60. Rows **a** and **b** show the same frames from different angles, where **b** is cut to focus on the internal structure. The black bar is a reference to the actual size of 10 grid points (gp).

and 9b for a comparison of their final stages), their formation process is much slower when compared to the unilamellar vesicles. Onion structures (Figure 9c) are formed via a pathway, which differs at later stages from the one for unilamellar vesicles. First, a disklike platelet similar to the platelets in Figure 8a,b is formed but of larger size. When the platelet starts to bend, a second platelet assembles from amphiphiles in the concave side of the parent platelet (Figure 9c). The process of sculpturing from the inside proceeds by the formation of a platelet of a third generation, while the onion is slowly closing up. Only very few objects in the final snapshot, Figure 9a, completed that process; others proceed on an alternative pathway toward a lamellae stack. The object size distribution is broad, similar to one in the previous section; however, the contribution of intermediate sizes is more pronounced compared to the smallest sizes. The mean cluster size is 1.02 vol %.

Vesicle Fusion. The next stage of structure coarsening is vesicle fusion. This stage is much slower than vesicle formation. Figure 10a,b disclosures the nontrivial details of the process. When two vesicles approach each other, they form a stalk in the form of a cylindrical micelle. Many theoretical contributions have considered the physics of a stalk (see e.g. ref 32). Here, we provide the kinetics of the whole process, demonstrating a very nontrivial pathway after the stalk is formed. Namely, after this initial stage, a hole is formed first in one of the vesicles, and consequently in the opposite one, each close to the foot of the stalk. Then the stalk flattens and bends, surrounding both perforations. At the end the stalk eventually closes up forming a neck between the two vesicles and connecting their inner compartments. The new object retracts slowly to a spherical shape. Vesicle fusion assisted by hole-formation was only very recently confirmed experimentally and found in Monte Carlo and static calculations,[18,20] as well as in molecular dynamics.[14] These studies,[18,20] however, consider merging of small flat bilayer patches under applied stress, while the molecular dynamics simulation[14] considers fusion of two vesicles pushed into the contact. Here we demonstrate the nonbiased evolution of many fusion processes in one simulation box. By considering the dynamics, our results favor only one of the several fusion mechanisms accompanied by hole formation, proposed earlier in the literature.[18,20]

Toroids. Two competing kinetic processes (micro- and macrophase separation) lead to a much richer zoo of nanocapsules than only simple vesicles and onions. Several structures found earlier experimentally, and long seen as being just exotic and not fitting into any theoretical description, appear to fit perfectly in our phase space of nonequilibrium metastable structures controlled only by the degree of relative solvophobicity of the molecular blocks and the molecule architecture (Figures 11 and 12).

In the case of highly asymmetric molecules, the polymeric phase will tend to form cylinders instead of lamellae. Macrophase separation leads to soft confinement, and cylinders form concentric tori (Figure 12**a**–**d**). This is not an exotic situation, as it holds for different asymmetric molecules, **c** and **d**. Large simulation volumes are full of such structures (see Figure 11, left), similar to the situation with the onion vesicles in Figure 4. Similar structures have been observed experimentally but were considered being isolated exotic structures.[33] Our results suggest that they can be metastable. They can have defects, like broken tori **b** and **d**. In the case of very small structures, the planes of tori can be perpendicular to each other and form banana shapes **b** as the cylinders cannot close into tori. Structure **a** removes the doom of exoticism completely. It shows that torus nanocontainers like **d** are formed from nuclei like **a**, which is simply the smallest possible stack of two lamellar platelets. In contrary to the case of symmetric molecules, the platelets **a** have a geometrical shape of discocites, similar to the shape of red blood cells. The size distribution (Figure 11) is rather broad again with an overall shape being rather sensitive to molecular composition. With increasing molecular asymmetry, these microstructures will on average lead to a decrease in the nanocontainer size (see Figure 11, right). The mean cluster sizes are (a) 1.1, (b) 0.92, and (c) 0.38 vol %.

Comparative Minkowski Image Characterization. Figure 13 shows the time evolution of the free energy for all systems ($j = 2-6$). As expected, the free energy goes down for all systems and reaches a plateau value. Zooming into the plateau region shows that the free energy still very slowly goes down. The simulations are stopped at this point in a view of time limitations.

We are aiming at describing systems in a large simulation volume. Our method gives the free energy of the system as a whole and is not well suited to provide specific contributions for separate structures in parts of the system, like, for instance, the bending energies of a particular object. The segregation parameters (Figure 14), in turn, provide information on an averaged segregation evolution for the different molecular species (hydrophobic, hydrophilic, and solvent) in the system but do not provide quantitative information about the shapes and microstructure topology. For all systems and all components the time pattern is the same—initial fast phase separation is followed by a long and slow plateau-like period of intensification of microinterfaces combined

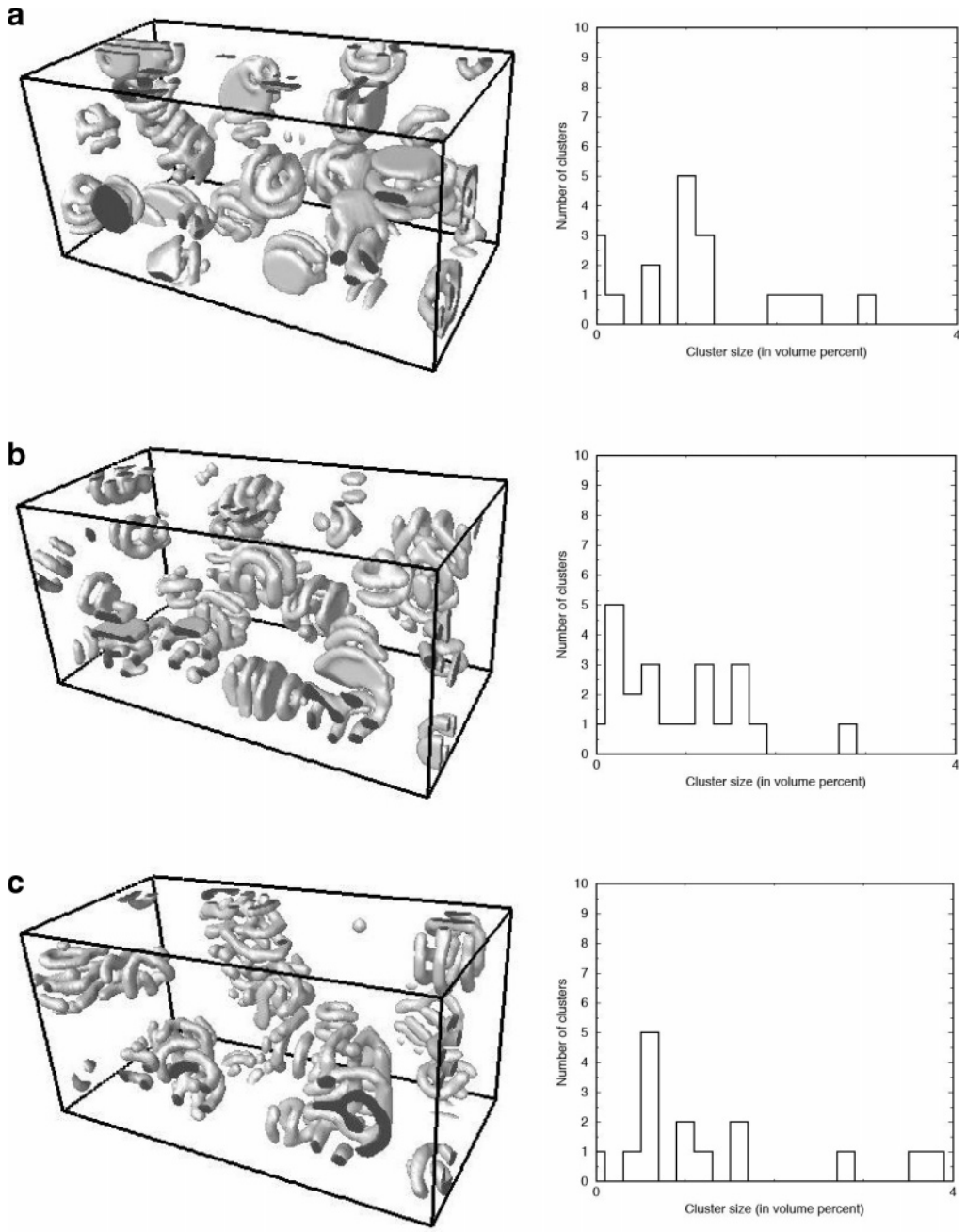

Figure 11. (left) Simulation result after 10^4 TMS of (a) system of 20% A_2B_4 amphiphile, (b) system of 20% A_2B_5 amphiphile, and (c) system of 20% A_2B_6 amphiphile, all in solvent. (right) Number of clusters vs cluster size, in percent of the total simulation volume, for the referring systems at the left side (10^4 TMS).

with structure rearrangement. The plots for the solvent are hardly distinguishable from each other, as the interaction with the solvent is kept the same for all systems. The difference between the A and B components is only due to different volume fraction in different system (the segregation parameter is not normalized to unity).

Nevertheless, there are other integral measures that can provide substantial additional insight on topological evolution details—we use the so-called Minkowski functionals (MF).[34] In three dimensions, three of the MF are related to the familiar geometrical quantities of (integrated) volume, surface area, and mean curvature. The fourth MF is the Euler characteristic χ, which is a measure for the topology, and can be understood as the number of connected components minus the number of tunnels (holes) plus the number of cavities. For instance,

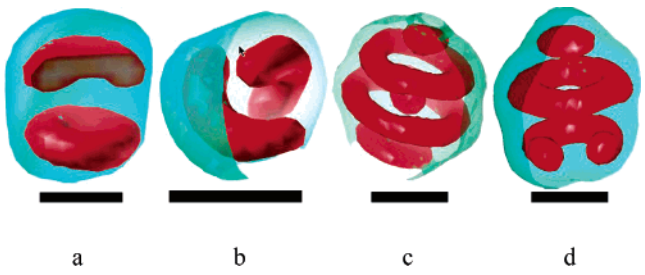

Figure 12. Zoo of nanocontainers (red, A-blocks; blue, B-blocks) obtained from simulating 20% amphiphile in a solvent. The structures show selected regions from a 128 × 64 × 64 box after 10^4 TMS for different amphiphiles: **a**–**c**, A_2B_5; **d**, A_2B_6. The B-isosurfaces are cut. Additionally, in (**a**) the A-isosurface is cut in the top part. Not mentioned parameters are the same as in Figure 4. The black bar is a reference to the actual size of 10 grid points (gp).

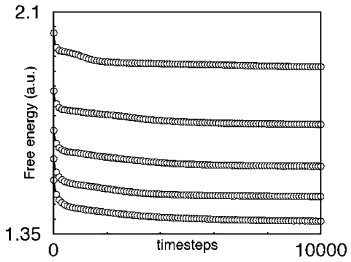

Figure 13. Combined free energy for all large simulation volumes under consideration.

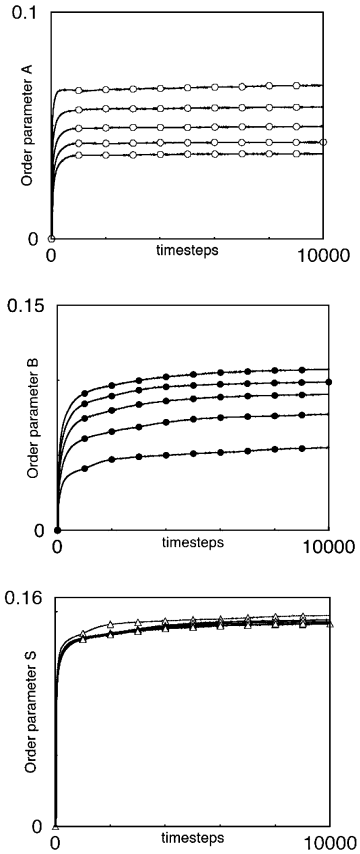

Figure 14. Combined evolution of the segregation parameters (top, hydrophobic A-block; middle, hydrophilic B-block; bottom, S-solvent) for all large simulation volumes under consideration.

$\chi = 1$ for a solid sphere, $\chi = 2$ for a hollow sphere, $\chi = 0$ for a torus, and $\chi = -1$ for a ∞-shape which has two holes. The Euler characteristic is related to the (intergrated) Gaussian curvature. Because of the additivity of the Minkowski functionals, we can use this knowledge for the determination of the topology of the majority part of the structures from the Euler characteristic. Figure 15a shows the time evolution of the MF (for a value of the threshold h_{tresh} equal to the mean density value of A in a concentrated amphiphilic region, i.e., $h_{\text{tresh}} = 0.5$ ($j = 2$), 0.4 ($j = 3$), and 0.25 ($j = 6$)) for the three chosen systems of most interest, containing mostly vesicles, onions, and toroids at the final stage.

The initial value of the Euler characteristic of Figure 15a is highly positive in all cases, indicating an initial situation of mostly spheres. In the remainder we use the terminology of spheres, but these can well be short cylinders or mixtures of short cylinders and spheres, as there is no topological distinction between spheres and short cylinders. The value of the Euler characteristic for a single sphere or truncated cylinder is one; the true shape can be deduced from the other MF values, like surface area and mean curvature, together with the absolute value of the Euler characteristic, which, for a collection of spheres, is equal to the total number of spheres. The higher initial Euler characteristic for $j = 3$ and 6 (see Figure 15b) is due to the fact that for $j = 2$ spheres start to merge into short cylinders at an earlier stage than for the other two, giving rise to a decrease in the Euler characteristic after already 200 TMS. A first conclusion, which one can draw from the graphs in Figure 15a, is that the curves for $j = 2$ and $j = 3$ overlap until ∼1000 TMS, showing similar topological behavior at the first stage of transformation. Indeed, both systems form vesicles following a sphere−cylinder−platelet−vesicle transformation. The topological evolution for both systems is similar until the onset of platelet bending for $j = 2$ (see also Figure 8). At about 1000 TMS, the Euler characteristic for $j = 2$ experiences a steeper drop for a short period and therefore decreases faster than the one for $j = 3$: this is the stage of platelet formation for $j = 2$. Therefore, we conclude that the system of shorter molecules, $j = 2$, forms platelets at an earlier stage. After that stage, the Euler characteristics of the system with $j = 2$ levels of into a plateau region, reflecting the fact that coarsening of the structures is mostly finished. Only their shape is changing by platelet bending and closing into vesicles. This plateau value is also an indication that this system ($j = 2$) never reaches the equilibrium morphology of a stack of lamellar sheets (with Euler characteristic equal to the number of sheets and therefore much smaller than the plateau value) within accessible simulation time: it is examplary for the fact that the structures obtained in this study are mostly nonequilibrium. The system of larger molecules, $j = 3$ (for which the end situation is that of vesicular structures, just like in the case of the symmetric system, $j = 2$), demonstrates a further drop in the Euler characteristics. This means that larger objects are created as the structure coarsening continues. The total amount of these objects in a fixed volume is smaller, so the Euler characteristic is lower. Figures 8 and 9c indeed confirm that the platelets in the system with $j = 3$ grow larger in size before closing into vesicles. Note that both cylinders and platelets are topologically identical to spheres and have the same Euler characteristic. The slightly negative value for $j = 3$ highlights the structural properties shown in Figure 8: almost all structures are defected onions—these are onions that have not yet closed up completely. The system consists of mostly bended platelets connected by necks, which are topologically seen as one sphere, but the total number will be small due to the large platelet volume. Moreover, their positive contribution to the Euler characteristic is mostly canceled by the negative contribution of holes in the platelets, which are obviously present at this stage of microstructure evolution. The behavior of the Euler characteristic for $j = 6$ is different: it starts with a similar high value as the other curves, indicating spheres as the starting structure, but falls off much slower in time than the other curves. This is not surprising for an inherently cylindrical system, which differs from the other systems ($j = 2$ and $j = 3$) in the sense that in the latter systems the cylinders are only transition structures between spherical micelles and

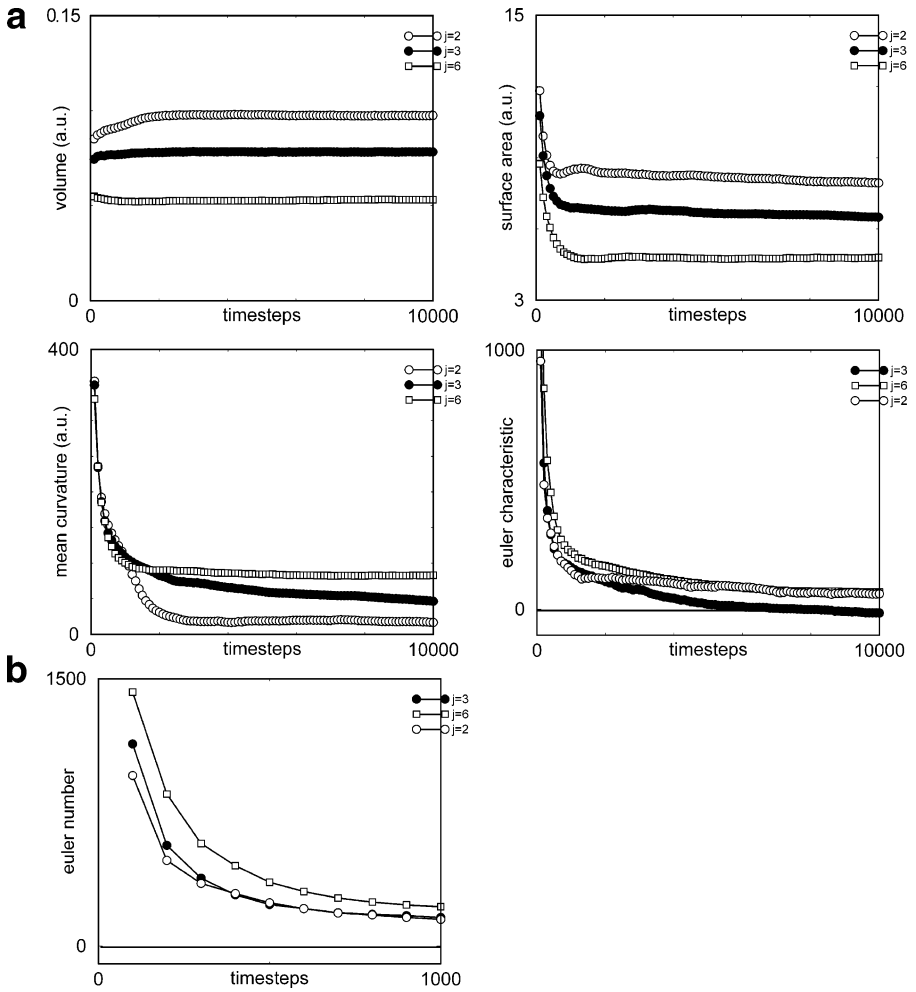

Figure 15. (a) Minkowski functionals for the A-block (threshold 0.5) as a function of time for the systems of 20% A_2B_2, A_2B_3, and A_2B_6 amphiphile in solvent (the final snapshots after 10^4 TMS is shown in Figures 4, 9a, and 11c). (b) Details of the Euler characteristic for the A-block (threshold 0.5) from (a).

platelets. The relatively low rate of the sphere-to-cylinder transition for $j = 6$ may have to do with frustration: there is a competition between the shape of the nanocontainers and the microstructure. To fit into the nanocontainers the cylinders have to bend, which is an undesirable situation for a cylinder. The shallow and steady slope of this curve reflects the few closing events of individual cylinders upon themselves in order to form tori (which lowers the Euler characteristic). An apparent plateau is reached for both $j = 2$ and 6: it even has a similar value. This is rather a coincidence due to similar number of objects (mostly seen as spheres) in both cases and has no particular deeper meaning. Just like for $j = 2$, where the vesicles are formed and further coarsening only takes place on a very long time scale (beyond the simulation), the rate at which cylinders close into tori is very slow, leading to an apparent saturation of the effect of this mechanism in the Euler characteristic. As the Euler number stays positive, we conclude that most cylinders are not yet totally closed to tori, which is well confirmed by the image shown in Figure 11a.

To make the analysis of the transformation dynamics complete we consider the other MF as well.

The time evolution of the volume shows that all systems are fully phase separated after ~2000 TMS; the rest of the morphological transitions take only place by rearrangements of the material. The difference in initial volume values is due to a different amount of minority component for the considered molecular composition (the total amount of polymeric surfactant is the same). The increase in the initial stages for $j = 2$ and 3 is the result of progressing microphase separation, as these systems are weaker segregated compared to $j = 6$ due to shorter chains, and therefore the value of χN is smaller. The system with the shortest chain shows the longest period of volume saturation, even longer then indicated in the segregation parameter evolution in Figure 14. The fact that the volume for $j = 6$ slightly goes down at the very beginning is an effect of the choice of the threshold value and is explained by the fact that the system initially consists of a mixture of spheres with weaker and stronger phase separation, which volume-wise are seen as the same (due to the thresholding procedure). While time progresses the weaker phase-separated spheres melt and eventually provide the material for the remaining spheres to grow into the cylindrical and torroidal structures.

The evolution of the surface area shows a general trend of decrease in time, indicating a positive surface tension for all systems. During the whole evolution, the surface area for $j = 2$ is higher than for $j = 3$, which in turn is higher than for $j = 6$. This difference exist even at very early stages, when all systems are spherical micelles; therefore, the difference in the degree of phase separation plays a role. There is a slight increase in

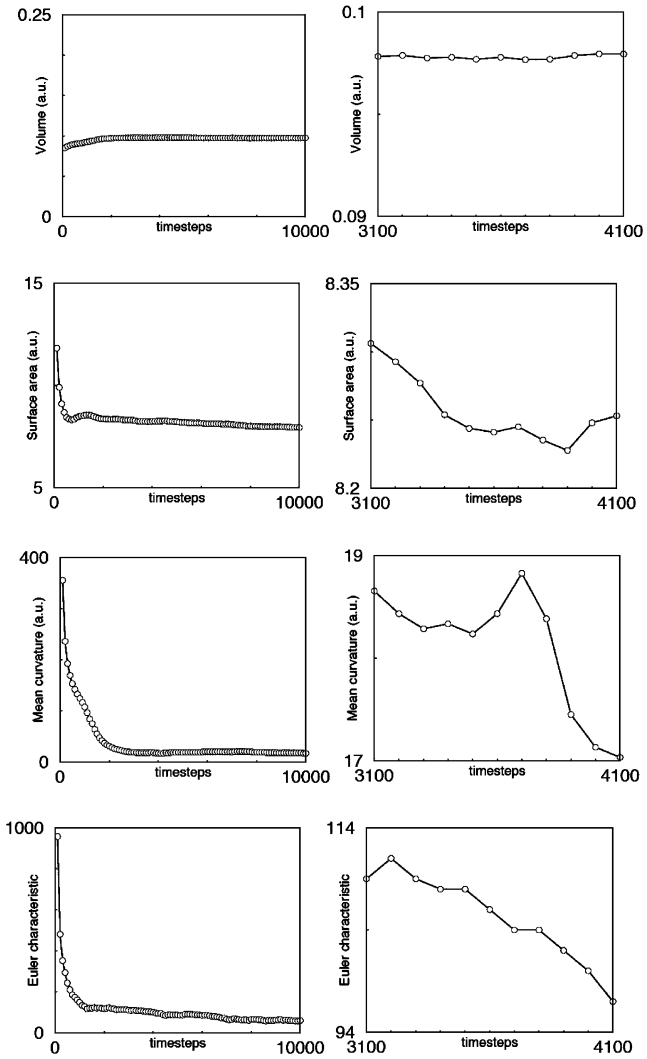

Figure 16. Minkowski functionals for the A-block (threshold 0.5) as a function of time for the system of 20% A_2B_2 amphiphile in solvent (the final snapshot after 10^4 TMS is shown in Figure 4). Left: whole simulation. Right: detail during vesicle fusion.

surface area (and therefore the associated energy) for $j = 2$, indicative of the fact that the surface contribution cannot be a leading contribution in the total energy of the system. So, the surface tension itself should be small, which is always the case for any real surfactants forming vesicles. To be precise, this contribution is small compared to curvature, as the curvature goes down and the overall energy should also go down. This increase in surface seems to be a combination of several factors. It takes place at the onset of the platelet-closing, where the formation of steeper gradients in the system still continues (as the plateau in volume is not yet reached), and well before the region where the formation of stalks and holes in platelets sets in (as the Euler characteristics is still considerably falling down at this stage). A considerably smaller surface area increase is also present for longer chains ($j = 3$) but at a later stage (around 4000 TMS) when compared to $j = 2$, which is a consequence of the increased platelet radius leading to a deferred bending onset for this system.

The general conclusion from the evolution of the mean curvature is that they are decreasing in time, indicating that for all systems the processes are curvature driven. Initially the curvatures are all roughly the same value; the process starts from spheres. For $j = 6$, these spheres transform into cylinders (tori) and stay this way starting from 2500 TMS. For $j = 2$, cylinders transform into objects of lower curvature (platelets and consequently vesicles). The mean curvature reaches a plateau value at a later stage compared to $j = 6$, as it corresponds to the region of vesicles, which comes to play later. For $j = 3$, the behavior of the mean curvature is qualitatively similar to $j = 2$, but it does not reach a plateau value. As we have shown before, most of the platelets are still in the process of closing up. Although the objects are larger than for $j = 2$, the presence of open edges gives rise to higher curvature compared to $j = 2$.

All the above analysis points at two phenomena: (1) Both systems with $j = 2$ and $j = 3$ experience a sphere−cylinder−platelet−vesicle transition. The mechanism is mainly *curvature* driven. The critical size of the platelets (the size at which the rim forces them to close up) is apparently much smaller for $j = 2$ than for $j = 3$. Also, the pathway is different: for $j = 2$ small vesicles merge to form larger vesicles, while for $j = 3$ large vesicles are formed in a single step by the "sculpturing from inside" process. (2) As we increase the asymmetry in the molecular architecture ($j = 6$), the transition halts in the cylindrical domain, and the system has the difficult task of packing the cylinders in larger cylindrical or spherical nanocontainers, leading to frustration and eventual formation of closed cylinders or tori.

The last remark should be made about vesicle fusion. Although the whole evolution seems to be mostly curvature driven, the fusion itself seems to be a complex interplay of all contributions to the free energy of the system. In Figure 16 we zoom into the Minkowski measures for the A_2B_2 system from Figure 5 around the time of two vesicles fusion, the structural details of which are depicted in Figure 10. There is no noticeable change of the system volume, so the phase separation is already finished at this stage and not changing. The mean curvature increases precisely at the moment of fusion, which is very understandable due to creation of both the sharper edges at the stalk and the perforations. This increase is counterbalanced by other contributions from the slight decrease of the surface area and the Gauss curvature (related to Euler number).

Conclusion

To conclude, we have simulated the entire process of vesicle formation and fusion starting from a complete mixture for a set of model amphiphiles and solvent. By systematically considering the effect of the free parameters, we show that self-assembly of many types of vesicles (found earlier in experiments and some believed to be exotic) forms a natural part of a unified evolution story. Simulating large systems on parallel machines minimizes the effect of boundary conditions. These conditions were found to be decisive for the description of processes, as subtle as the ones set forth, for the first time.

Acknowledgment. Stichting Nationale Computer Faciliteiten (NCF) is acknowledged for providing computer time on the Teras Supercomputer at SARA (Amsterdam).

Supporting Information Available: A movie showing the complete vesicle evolution of the system shown in Figure 4. This material is available free of charge via the Internet at http://pubs.acs.org.

References and Notes

(1) Lasic, D. D. *Nature (London)* **1991**, *351*, 613.
(2) Leng, J.; Egelhaaf, S. U.; Cates, M. E. *Europhys. Lett.* **2002**, *59*, 311−317.
(3) Leng, J.; Egelhaaf, S. U.; Cates, M. E. *Biophys. J.* **2003**, *85*, 1624−1646.
(4) Lipowsky, R. *Nature (London)* **1991**, *349*, 475−481.
(5) Lentz, B. R.; Malinin, V.; Hague, M. E.; Evans, K. *Curr. Opin. Struct. Biol.* **2000**, *10*, 607−615.
(6) Zimmerberg, J.; Chernomordik, L. V. *Adv. Drug Deliv. Rev.* **1999**, *38*, 197−205.
(7) Cameron, N. S.; Corbierre, M. K.; Eisenberg, A. *Can. J. Chem.* **1999**, *77*, 1311−1326.
(8) Discher, D. E.; Eisenberg, A. *Science* **2002**, *297*, 967−973.
(9) Drouffe, J.-M.; Maggs, A. C.; Leibler, S. *Science* **1991**, *254*, 1353−1356.
(10) Bernardes, A. T. *Langmuir* **1996**, *12*, 5763−5767.
(11) Noguchi, H.; Takasu, M. *Phys. Rev. E* **2001**, *64*, 041913.
(12) Yamamoto, S.; Maruyama, Y.; Hyodo, S. *J. Chem. Phys.* **2002**, *116*, 5842−5849.
(13) Benardes, A. T. *J. Phys. II* **1996**, *6*, 169−174.
(14) Marrink, S. J.; Mark, A. E. *J. Am. Chem. Soc.* **2003**, *125*, 15233−15242.
(15) de Vries, A. H.; Mark, A. E.; Marrink, S. J. *J. Am. Chem. Soc.* **2004**, *126*, 4488−4489.
(16) Noro, M. G.; Meneghini, F.; Warren, P. B. In *Mesoscale Phenomena in Fluid Systems*; Case, F., Alexandridis, P., Eds.; *ACS Symp. Ser.* **2003**, *861*, 242−257.
(17) Yamamoto, S.; Hyodo, S. *J. Chem. Phys.* **2003**, *118*, 7937−7943.
(18) Müller, M.; Katsov, K.; Schick, M. *J. Chem. Phys.* **2002**, *116*, 2342−2345.
(19) Noguchi, H.; Takasu, M. *J. Chem. Phys.* **2001**, *115*, 9547−9551.
(20) Müller, M.; Katsov, K.; Schick, M. *J. Polym. Sci., Part B: Polym. Phys.* **2003**, *41*, 1441−1450.
(21) Marrink, S. J.; Mark, A. E. *J. Am. Chem. Soc.* **2003**, *125*, 11144−11145.
(22) Shillcock, J.; Lipowsky, R. *Nat. Mater.* **2005**, *4*, 225−228.
(23) Szostak, J. W.; Bartel, D. P.; Luisi, P. L. *Nature (London)* **2001**, *409*, 387−390.
(24) He, X.; Liang, H.; Huang, L.; Pan, C. *J. Phys. Chem. B* **2004**, *108*, 1731−1735.
(25) van Vlimmeren, B. A. C.; Maurits, N. M.; Zvelindovsky, A. V.; Sevink, G. J. A.; Fraaije, J. G. E. M. *Macromolecules* **1999**, *32*, 646−656. Fraaije, J. G. E. M.; van Vlimmeren, B. A. C.; Maurits, N. M.; Postma, M.; Evers, O. A.; Hoffmann, C.; Altevogt, P.; Goldbeck-Wood, G. *J. Chem. Phys.* **1997**, *106*, 4260−4269.
(26) Morita, H.; Kawakatsu, T.; Doi, M.; Yamaguchi, D.; Takenaka, M.; Hashimoto, T. *Macromolecules* **2002**, *35*, 7473−7480.
(27) Hashimoto, T.; Sakamoto, N.; Koga, T. *Phys. Rev. E* **1996**, *54*, 5832−5835.
(28) Hashimoto, T.; Mitsumura, N.; Yamaguchi, D.; Takenaka, M.; Morita, H.; Kawakatsu, T.; Doi, M. *Polymer* **2001**, *42*, 8477−8481.
(29) Morita, H.; Kawakatsu, T.; Doi, M.; Yamaguchi, D.; Takenaka, M.; Hashimoto, T. *J. Phys. Soc. Jpn.* **2004**, *73*, 1371−1374.
(30) Burke, S. E.; Eisenberg, A. *Langmuir* **2001**, *17*, 6705−6714.
(31) Chen, L.; Shen, H.; Eisenberg, A. *J. Phys. Chem. B* **1999**, *103*, 9488−9497.
(32) Kozlovsky, Y.; Kozlov, M. M. *Biophys. J.* **2003**, *85*, 85−96.
(33) Zhang, L.; Bartels, C.; Yu, Y.; Shen, H.; Eisenberg, A. *Phys. Rev. Lett.* **1997**, *79*, 5034−5037.
(34) Sevink, G. J. A.; Zvelindovsky, A. V. *J. Chem. Phys.* **2004**, *121*, 3864−3873.

MA0506740